Chapter 3

Statistical Models of the Interstellar Medium

3.1 Introduction

The problem of modelling star formation in large scale simulations is a difficult one for a number of reasons. Firstly, the detailed process of star formation is not fully understood even in our own galaxy and additionally we expect that young galaxies in the high redshift Universe will have wildly differing properties from those of our own quiescent disk. Secondly, on the scales of interest in Cosmological simulations (tens of Mpc and upwards) we can not achieve the required spatial or mass resolution to resolve the actual formation of stars. Most star formation prescriptions in the literature today approach this in one of two ways. Either by creating a set of rules that govern when a 'gas unit' (be that particle or grid cell) may change into a star particle, then converting them in a stochastic manner (Kay et al. (2002)) or by describing the interstellar medium (ISM) in a statistical manner (Springel and Hernquist (2003); Yepes et al. (1997)). In the following chapter we introduce examples of the first generation of star formation models before discussing the major problems with them. We then describe in detail our own implementation of the physical processes that are important in star formation and the evolution of the ISM.

3.1.1 Models of Star Formation Using a Single Phase

The basic empirical law that most numerical models either use explicity or try to fit by the adjustment of free parameters is the Kennicutt law (Schmidt (1959)):

$$\Sigma_{SFR} = C\Sigma_{gas}^{N} \tag{3.1}$$

Where Σ denotes a density per unit area. This simple power law relation between star formation rate density (SFR) and gas density was found to hold over many orders of

magnitude by Kennicutt (1988), who constrained the exponent to be $N = 1.4 \pm 0.2$.

The basic process by which star formation is then modelled is to, at each timestep, apply some sensible criteria that describe whether or not a particular gas unit is eligible to turn into a star. Some criteria that have been used in the literature include (X represents a free parameter in each rule):

1. The minimum overdensity: $\delta > X$
2. The minimum physical density: $\rho > X$
3. The maximum temperatute: $T < X$
4. Converging flow: $\nabla.v < 0$
5. Jeans instability: $\tau_J < \tau_{dyn}$
6. Cooling instability: $t_{cool} < t_{dyn}$

Rules 1 and 2 prevent underdense material from collapsing and forming stars, rule 3 prevents material that is too hot to collapse gravitationally from turning into stars. Rule 4 represents the local estimate of the divergence of the gas flow, for example in an SPH simulation this is given by

$$\nabla.v_i = -\frac{1}{\rho_i}\sum m_j v_{ij}\frac{1}{2}\left[\nabla_i W(r_{ij}, h_i) + \nabla_i W(r_{ij}, h_j)\right] + \frac{H_i - \Lambda_i}{\rho_i}\,, \tag{3.2}$$

where $W(r, h)$ is the SPH kernel so $\nabla.W(r, h)$ is the direction of the gradient of the SPH kernel at a given point. A negative divergence represents a net flow of baryonic material into this mass unit.

Rule 5 forces that only material that is Jeans unstable (that is: it is unstable to any perturbations and cannot diffuse away density fluctuations as sound waves) to collapse. In a Lagrangian simulation a particle may be considered Jeans unstable if

$$\frac{h_i}{c_i} < \frac{1}{\sqrt{4\pi G\rho_i}}\,. \tag{3.3}$$

Here, h_i represents the SPH smoothing length of the gas particle, c_i is the sound speed in that particle.

The final rule represents the fact that as a gas cloud collapses it heats up. If the time it takes for a gas cloud to radiate away this extra heat is less than the characteristic timescale on which it can collapse then it can continue to collapse unimpeded; otherwise it will become pressure supported.

Table 3.1: Star formation criteria used by different authors

Author(s)	Star Formation Rules
Pearce et al. (1999) (see Kay et al. (2002))	$\delta > X$; $T < X$
Summers (see Kay et al. (2002))	$\delta > X$; $T < X$; $\rho > X$
Navarro and White (1993)	$\rho > X$; $\nabla.v < 0$; $t_{cool} < t_{dyn}$
Steinmetz and Mueller (1994)	$\nabla.v < 0$; $t_{cool} < t_{dyn}$; $\delta > X$
Katz (1992)	$\tau_J < \tau_{dyn}$; $\nabla.v < 0$; $t_{cool} < t_{dyn}$
Cen and Ostriker (1992)	$\delta > X$; $\nabla.v < 0$; $\tau_J < \tau_{dyn}$
Katz et al. (1996)	$\delta > X$; $\rho > X$; $\nabla.v < 0$
Mihos and Hernquist (1994b)	$\delta > X$; $\nabla.v < 0$

A selection of the particular criteria chosen by a number of authors is included in table 3.1.1. When some gas unit has been labelled as eligible to form stars by whatever set of rules its author has chosen then its SFR is calculated by the Schmidt law (equation 3.1), and then depending upon its SFR has some probability of either

- being converted into a collisionless star particle representing millions, or hundreds of millions of stars, or
- spawning a new collisionless star particle with a mass in direct proportion to the SFR of the gas particle and decreasing the mass of the gas particle by an equivalent amount

The first approach has the advantage that it is both simple to implement and actually cuts down on the amount of computational work that needs to be done on each timestep as more stars are formed (star particles do not feel hydrodynamic forces). On the other hand, the minimum amount of star formation that can be resolved is equal to the mass resolution of the simulation. The second approach has the advantage that smaller amounts of star formation can be resolved but it can be computationally very expensive to calculate gravitational forces after spawning a lot of new collisionless particles in high density regions.

A comparison of different star formation methods (including most of those in table 3.1.1) was recently undertaken by Kay et al. (2002) who found that although each prescription agreed well in most ways that some fundamental physical properties, such as the fraction of baryons in stars, in each simulation could vary greatly between star for-

mation treatments. The star formation histories for each method also showed significant differences in shape.

One of the largest problems with the modelling of star formation in this manner is that these star formation recipes are chosen purely phenomenologically and although they may mirror the large scale behaviours of star forming regions they offer no insights into the actual dynamic processes that go into the formation of stars.

Additionally feedback from core collapse (type II) SNe, described as an extra source of thermal or kinetic energy in these single phase models, was found to have little effect in the early models. This is because the gas in the surroundings of star formation sites is at high density and so is very efficient at just radiating away the added energy. As a consequence, too much gas cooled in dense knots, producing galaxies much more concentrated than those observed (Navarro and Benz (1991); Weil et al. (1998)).

3.1.2 Multiphase Star Formation

In response to these problems with the simplest star formation and feedback criteria several authors have introduced 'multiphase' models for star formation in which the ISM is treated as a number of distinct phases. These schemes take various forms including modification of the simulation algorithm (Ritchie and Thomas (2001); Croft et al. (2000)), treating the multiphase medium implicitly by formulating differential equations that model the interactions between the phases(Yepes et al. (1997); Springel and Hernquist (2003); Okamoto et al. (2005)), or by decoupling the cold molecular phase from the hot phase by means of 'sticky particles' (Semelin and Combes (2002); Harfst et al. (2006)), removing 'cold' particles from the SPH calculation (Hultman and Pharasyn (1999); Pearce et al. (1999, 2001); Marri and White (2003)), or by explicit modification of the SPH routines to decouple cold, molecular gas from the hot phase (Scannapieco et al. (2006)). The decoupling of the hot and cold ISM phases allows thermal heating from SN feedback to become more efficient (due to the much lower density of the hot phase), and also allows one to follow the properties of the cold molecular phase of the ISM. In this chapter we describe how the physical processes integral to the evolution of the ISM may be modelled computationally.

3.2 Details of the Sticky Particle Model

In typical simulations of galaxy formation we can resolve the Jeans length of the ambient gas phase and so can treat its hydrodynamic properties consistently. However, we cannot yet resolve the properties of the cold molecular phase of the ISM. We therefore follow the evolution of the ambient gas phase using a hydrodynamic simulation code, whereas we treat the cold phase using a statistical model that encapsulates the physics relevant to the formation and evolution of molecular clouds. In this section we introduce the properties of the sticky particle model and describe the physics we have implemented.

Following Efstathiou (2000) we consider the ISM to consist of warm and hot ambient materials, and cold molecular clouds. We additionally treat the properties of SN remnants. Throughout this chapter the properties of the ambient medium will be represented with the subscript h, the properties of the molecular clouds with the subscript c, and the properties of the gas internal to SN remnants, or hot bubbles, with the subscript b.

The ambient gas phase is represented using the entropy conserving, parallel Tree-SPH code GADGET2 (Springel (2005); Springel et al. (2001)). The properties of SPH simulation codes were introduced in some detail in chapter 2. We will refer to the gas component treated using SPH interchangeably as ambient, warm or hot, to distinguish it from the cold molecular gas. We will see that in galaxy formation simulations, this ambient (i.e. non-molecular) medium naturally develops three relatively well-defined phases: a warm ($T \sim 10^4$K) component in a galactic disk, a hot ($T \sim 10^6$K)) tenuous component of shock-heated gas in the halo, and a similarly hot component resulting from gas heated by SN. The fourth, cold ($T \sim 100$K) and molecular cloud phase is represented with sticky particles, which interact gravitationally with all other material in the simulation and are allowed to stick together forming more massive sticky particles. Stars and dark matter are both treated as collisionless particles by GADGET2.

The different phases of the ISM may interact with each other as follows: thermally unstable ambient gas may collapse into molecular clouds via thermal instability (section 3.2.1). Molecular clouds can interact with each other to form GMCs (section 3.2.2). GMCs then collapse into stars (section 3.2.5). Stars disrupt the cloud they formed from and may, via SN feedback, return energy (section 3.2.6) to the ambient phase. Hot bubbles blown by SNe can evaporate cold clouds (3.2.7) and heat the ambient medium.

Fig 3.1 contains a summary of all of the physics implemented in our model. Arrows

represent a transfer of mass and/or energy from one phase to another. The distinction between clouds and GMCs is somewhat arbitrary; they are separated in the figure to allow an easy pictorial representation of mass and energy transfer within a single phase. Appendix A contains a list of frequently used symbols and their meaning.

Each physical process will be treated in turn in the remainder of this section. We first introduce the physics relevant to each physical process before discussing the numerical implementation. We will also give our preferred physical values for the various parameters that occur. How we choose these is discussed in section 3.3.

3.2.1 Radiative Cooling And The Formation of Molecular Clouds

Begelman and McKee (1990) show that under appropriate physical conditions, a thermal instability may operate in hot gas which causes a fraction of the gas to condense into much colder molecular clouds. The sticky particle star formation prescription contains a basic representation of this process, based on a detailed treatment of baryonic radiative cooling.

Relevant Physics

The radiative processes that we take into account are Compton cooling off the microwave background, thermal Bremsstrahlung cooling, line cooling and photo-ionization heating from Hydrogen, Helium and metal species in the presence of an imposed ionising background. These routines were developed for a different project and will be described elsewhere[1]. Briefly, they use tabulated rates for radiative cooling and photo-ionization heating for many species and ionization states computed assuming ionization equilibrium using CLOUDY (version 05.07 of the code last described by Ferland et al. (1998)) with a UV background given by Haardt and Madau (2001). The rates are tabulated element by element and we will assume solar abundance ratios and specify a fixed metallicity of the gas in solar units. We do, however, note that the behaviour of the system may depend upon precisely which value of the metallicity we choose, and investigate this in section 4.4

Other processes such as cosmic ray heating, and cooling by dust and atomic lines that affect the molecular gas in clouds are not treated explicitly since we do not model the internal properties of the clouds themselves.

[1]We would like to thank our colleagues J Schaye, C Dalla Vecchia and R Wiersma for allowing us to use these rates.

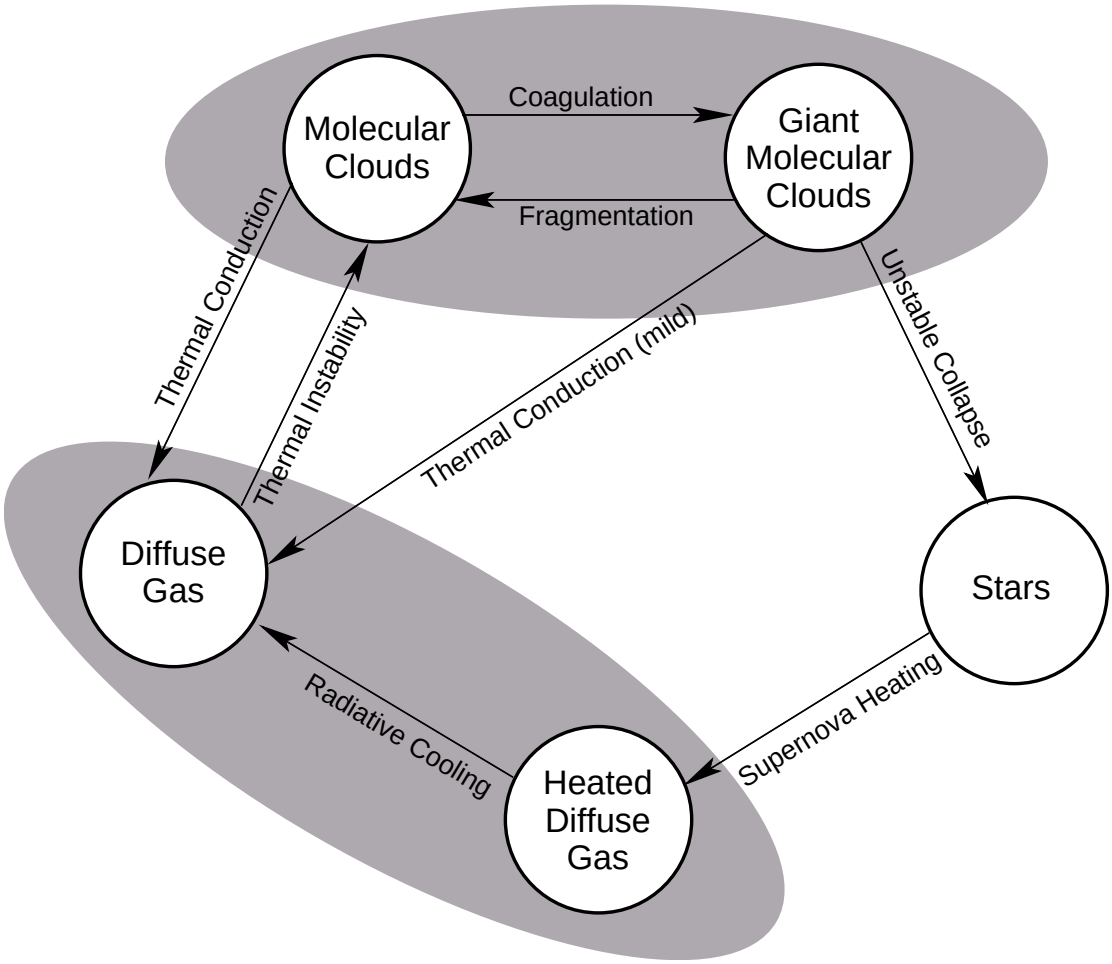

Figure 3.1: Summary of the physical processes that operate in our model of a two phase interstellar medium. The boundaries between molecular and giant molecular clouds and between heated and non-heated diffuse gas are somewhat arbitrary and they are separate out in this figure only to highlight the different physical mechanisms that are operating at any given time. Each arrow represents the transfer of mass and/or energy from one phase to another.

We include a simple model to determine the rate at which the ambient gas forms molecular clouds. When we identify ambient gas that is thermally unstable (Begelman and McKee (1990)) we allow it to collapse into molecular clouds. The rate at which this process occurs is goverened by the rate at which the gas is losing thermal energy by radiative cooling.

Numerical Implementation

Following Yepes et al. (1997) we define a density threshold, $\rho_{\rm th}$, to determine when gas becomes thermally unstable. Gas with $\rho < \rho_{\rm th}$ undergoes ordinary radiative cooling. Gas with density above the threshold becomes thermally unstable and begins to be converted to molecular clouds. In addition to the density criterion we add a maximum temperature ($T_{\rm th}$) for gas to be called thermally unstable which has the effect of preventing SN heated gas in dense regions from collapsing straight to the cold phase.

When gas has been identified as thermally unstable it begins to form molecular clouds at a rate controlled by the rate at which the gas can lose thermal energy by radiative cooling

$$\frac{d\rho_c}{dt} = -\frac{d\rho_h}{dt} = \frac{1}{u_h - u_c}\Lambda_{\rm net}(\rho_h, u_h), \tag{3.4}$$

where u_h and u_c represent the internal energies per unit mass of the ambient phase and cold phase respectively and $\Lambda_{\rm net}$ is the cooling rate of the ambient gas (ergs cm^{-3} s^{-1}). We assume that the cold clouds remain at a fixed temperature of $T_{\rm c} = 100$K hence their thermal energy $u_{\rm c}$ is a constant as well.

In practice, each ambient gas particle is identified as either thermally unstable, or non-thermally unstable. Non-thermally unstable gas undergoes radiative cooling; thermally unstable ambient gas forms molecular clouds at a rate controlled by the radiative cooling rate, as described by Eq. 3.4.

In this way each ambient gas particle can keep track of what fraction of its mass is in the form of molecular clouds. Gas in the molecular phase is ignored for the purposes of the SPH calculation. When the amount of mass in the molecular phase in a particle reaches the resolution limit of the simulation a seperate 'sticky particle', representing many sub-resolution molecular clouds is created. This process decouples the molecular clouds from the associated ambient phase. Since we cannot resolve the individual molecular clouds in each sticky particle we work with the mass function of clouds. Initially we assume that the molecular clouds formed through instability are all in the smallest mass

bin, that is that the clouds formed by thermal instability are very small, and will interact to form more massive clouds. In the following section we describe the behaviour and evolution of the sticky particles in the simulation.

3.2.2 Cloud Coagulation and GMC Formation

Molecular clouds are typically many orders of magnitude more dense than the medium they form in (MO77), and their behaviour is governed by a different set of rules than the ambient medium. This section describes the physics of the simplified molecular clouds in the sticky particle model and how it is implemented.

Relevant Physics

We assume that clouds may be treated as approximately spherical objects that obey a power law relation between mass (M_c) and radius (r_c)

$$\begin{aligned} r_c &= \left(\frac{M_c}{M_{\rm ref}}\right)^{\alpha_c} r_{\rm ref} \\ &= 36 \left(\frac{M_c}{10^5 M_\odot}\right)^{0.3} {\rm pc}\,. \end{aligned} \tag{3.5}$$

Here, α_c describes how clouds grow as mass is added to them (if they remain at constant density then $\alpha_c = 1/3$), and $M_{\rm ref}$ and $r_{\rm ref}$ are a reference mass and radius used to fix the normalisation of this relation. The example phyical values used in this equation are discussed fully in section 3.3.1. The lower bound on molecular cloud masses is typically calculated to be $100 M_\odot$ (Monaco (2004)) due to the efficient destruction of smaller molecular clouds by photoionization. We introduce an upper limit by converting molecular clouds with large masses into stars (see section 3.2.5 for discussion). In order to facilitate easy estimates of the relative importance of various effects we have substituted typical numbers and units into most of the equations in this section.

Numerical Implementation

Each sticky particle represents numerous cold clouds. Sticky particles are hydrodynamically decoupled from the ambient SPH phase of the gas and interact only gravitationally with the other phases in the simulation. However, when two sticky particles collide they may coagulate to form a more massive sticky particle. The mass of the smallest molecular clouds is typically orders of magnitude below the mass resolution in a cosmological simulation. We represent an entire mass spectrum of clouds statistically inside of each

sticky particle. Our formalism to treat the evolution of the mass function of clouds internal to each of the 'multiple cloud' particles will start from the Smoluchowski equation of kinetic aggregation (Smoluchowski (1916)), which describes the behaviour of a system consisting of ballistic particles that can interact via mergers. The coagulation behaviour of this system is driven by a coagulation kernel, $K(m_1, m_2)$, that represents the formation rate of clouds of masses $m = m_1 + m_2$,

$$K = \langle \Sigma v_{\rm app} \rangle_v, \tag{3.6}$$

where $v_{\rm app}$ is the relative velocity of the clouds and Σ is the collision cross section. For a Maxwellian distribution of velocities with three-dimensional dispersion σ we have $\langle v_{\rm app} \rangle = 1.3\sigma$ (Monaco (2004)). The product of the approach velocity and the collision cross section is averaged over the distribution of relative velocities. The cross section is

$$\Sigma \approx \pi (r_c + r_c')^2 \left(1 + 2G \frac{M_c + M_c'}{r_c + r_c'} \frac{1}{v_{\rm app}^2}\right), \tag{3.7}$$

where the first term represents the collision geometric cross section and the second term represents the effect of gravitational focusing (Saslaw (1985)). The focused term becomes significant when the approach velocity is not much larger than the internal velocity dispersion of the system. In most cases of interest the geometric term will dominate so the focused term is neglected. In these calculations we need to assume that molecular clouds, although transient and turbulent, are stable for long enough for coagulation to take place. This is reasonable because the cloud velocity dispersion is typically larger than the sound speed of the cold cloud gas (Monaco (2004)).

To model the cooling of sub-resolution molecular clouds via gravitational interaction it has been assumed that when molecular clouds with relative velocities, $v_{\rm app}$, greater than $v_{\rm stick}$ (a parameter in our simulations) collide they do not merge, but rather bounce back with relative velocity a fraction, η, of the initial approach velocity. Clouds with relative velocities less than $v_{\rm stick}$ merge. For simplicity it has been assumed that the velocity distribution of clouds is Gaussian with a velocity dispersion that is a function of cloud mass, $\sigma = \sigma(m)$.

The upper and lower bounds on the molecular cloud mass function are set such that the smallest mass bin is comparable with the smallest observable clouds, and the largest molecular clouds are approximately the same mass as the largest clouds in the MW. The mass function is discrete. All clouds are assumed to form at the lowest mass, M_{min},

and then the mass of each bin is a multiple of this value. This discrete mass function is neccessary when working with the Smoluchowski equation.

In order for us to be able to hold a mass function with a large number of bins internal to every single sticky particle without the requirement to store one number for each mass bin we parameterize the mass function as a third order polynomial, and store only the four coefficients between timesteps.

As these sub-resolution clouds interact and merge, the one dimensional velocity dispersion $\sigma(m)$ changes, which affects the rate of evolution of the cloud mass function, $n(m)$. Let $E_{\rm m} = (3/2)m\sigma^2(m)$ denote the random kinetic energy of clouds with mass m. $E_{\rm m}$ may change due to three distinct processes:

- Clouds with masses m' and $m - m'$ merge to form extra clouds of mass m, increasing $E_{\rm m}$ at a rate $\dot{E}_{\rm gain}$
- Clouds with masses m may merge with clouds of any other mass decreasing the number of clouds of mass m. This process decreases $E_{\rm m}$ at a rate $\dot{E}_{\rm loss}$
- Clouds with mass m may interact collisionally with clouds of any other mass and so lose kinetic energy. This process decreases $E_{\rm m}$ at a rate $\dot{E}_{\rm cool}$

The net change in kinetic energy for particles of mass m during some timestep Δt is given by

$$\Delta E_m = \frac{dE_m}{dt}\Delta t = \left[\dot{E}_{\rm gain} - \dot{E}_{\rm loss} - \dot{E}_{\rm cool}\right]\Delta t\,. \tag{3.8}$$

And for this change in kinetic energy, the corresponding change in velocity dispersion is given by

$$\dot{\sigma} = \frac{2\dot{E} - \dot{M}\sigma^2}{2M\sigma}\,. \tag{3.9}$$

Details of the equations used to model these processes are given in Appendix 3.2.3, and the method by which they are solved numerically in Appendix 3.2.4.

The same processes (cooling and merging) are followed explicitly for the individual sticky particles in our simulations, which can interact in the same two ways as the unresolved sub resolution clouds. Following the same rules should allow us to remove much of the resolution dependence of the star formation. As the mass resolution of a simulation is degraded, more massive clouds will be treated with the sub-grid physics; our implementation should ensure that the large scale results are approximately the same. This is demonstrated in section 3.3.1.

3.2.3 Energy Transfer Through Coagulation

In this section the numerical methods by which the equations governing molecular cloud behaviour are discussed in detail. The starting point is the Smoluchowski equation of kinetic aggregation (Smoluchowski (1916))

$$\frac{\partial n}{\partial t} = \frac{1}{2V}\int_0^\infty n(m',t)n(m-m',t)K(m',m-m')dm' \\ -\frac{1}{V}n(m,t)\int_0^\infty n(m',t)K(m,m')dm', \tag{3.10}$$

where $n(m,t)$ represents the number of clouds with masses between m and $m+dm$ contained within a volume, V and $K(m,m')$ represents the kernel for aggregation of clouds with masses m and m', as defined by Eq (3.6)

In one dimension, the fraction of collisions between clouds of masses m_1 and m_2 that lead to mergers is given by

$$f_m(\sigma_1,\sigma_2) = \frac{1}{\sigma_1\sqrt{2\pi}}\int_{-\infty}^{\infty} e^{-\left(\frac{v_1}{\sqrt{2}\sigma_1}\right)^2}\Big[\mathrm{erf}\big(\frac{v_1+v_{\mathrm{stick}}}{\sqrt{2}\sigma_2}\big)-\mathrm{erf}\big(\frac{v_1-v_{\mathrm{stick}}}{\sqrt{2}\sigma_2}\big)\Big]dv_1\,. \tag{3.11}$$

Figure 3.2 shows for two populations of particles with different velocity dispersions the fraction of collisions that will lead to a merger, this demonstrates the symmetry between σ_1 and σ_2 in equation 3.11. Using this definition of f_{m} the Smoluchowski equation becomes

$$\frac{\partial n}{\partial t} = \frac{1}{2V}\int_0^\infty n(m',t)n(m-m',t)K(m',m-m')f_m(\sigma_{m'},\sigma_{m-m'})dm' \\ -\frac{n(m,t)}{V}\int_0^\infty n(m',t)K(m,m')f_m(\sigma_m,\sigma_{m'})dm'\,. \tag{3.12}$$

As discussed in section 3.2.2, clouds of mass m may gain or lose kinetic energy in three ways: clouds of mass m' and $m-m'$ may merge to form extra clouds of mass m. Clouds of mass m may merge with clouds of any other mass to decrease the number of clouds of mass m. Finally clouds of mass m can interact gravitationally with any other clouds, thus losing kinetic energy. These three processes are termed gain, loss and cooling.

Gain processes may be represented in the following way, where we have integrated over m' such that the two particles that merge have masses that sum to m

$$\dot{E}_{\mathrm{gain}} = \int_0^\infty\int_{v_1=-\infty}^{v_1=\infty}\int_{v_2=v_1-v_{\mathrm{stick}}}^{v_2=v_1+v_{\mathrm{stick}}}\Big[P(v_1)P(v_2)n(m',t) \\ n(m-m',t)K(m',m-m')f_m(m',m-m')E_f\Big]dv_2dv_1dm'\,. \tag{3.13}$$

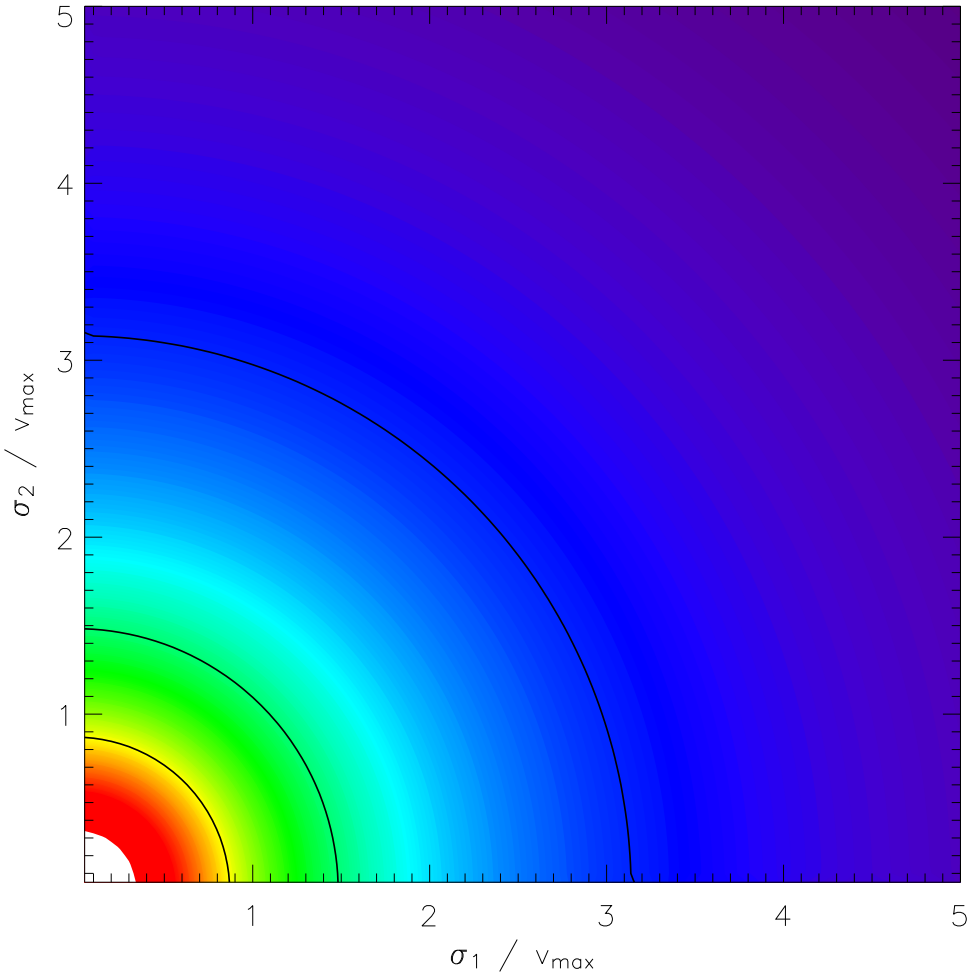

Figure 3.2: The merging fraction as a function of σ_1 and σ_2. White represents a merging fraction of 1.0, dark blues represent low merging fractions. The solid black lines show merging fractions of 0.75, 0.5 and 0.25.

$P(v_1)$ and $P(v_2)$ are the probability distributions velocities v_1 and v_2 and are assumed to be gaussian with standard deviation σ_1 and σ_2 respectively. E_f represents the final kinetic energy of a collision between particles of masses m' and $m - m'$. E_f is evaluated by considering conservation of momentum,

$$E_\mathrm{f} = \frac{1}{2}\frac{(m'v_1 + (m-m')v_2)^2}{m}\,. \tag{3.14}$$

Eq (3.13) then becomes

$$\begin{aligned}\dot{E}_\mathrm{gain} = \frac{n(m',t)}{2\pi}\int_0^\infty n(m-m',t)K(m',m-m')\\ \int_{-\infty}^{\infty}\int_{v_1-v_\mathrm{stick}}^{v_1+v_\mathrm{stick}}\frac{1}{\sigma_{m'}\sigma_{m-m'}}e^{-\left(\frac{v_1}{\sqrt{2}\sigma_{m'}}\right)^2}e^{-\left(\frac{v_2}{\sqrt{2}\sigma_{m-m'}}\right)^2}\\ \frac{1}{2}\Big(\frac{(m'v_1+(m-m')v_2)^2}{m}\Big)dv_2dv_1dm'\,,\end{aligned} \tag{3.15}$$

and Eq (3.15) may be written

$$\begin{aligned}\dot{E}_\mathrm{gain} = \frac{n(m',t)}{2\pi}\int_0^\infty n(m-m',t)K(m',m-m')\int_{-\infty}^{\infty}\frac{1}{\sigma_{m'}\sigma_{m-m'}}e^{-\left(\frac{v_1}{\sqrt{2}\sigma_{m'}}\right)^2}\\ \int_{v_1-v_\mathrm{stick}}^{v_1+v_\mathrm{stick}}e^{-\left(\frac{v_2}{\sqrt{2}\sigma_{m-m'}}\right)^2}\frac{1}{2}\Big(\frac{(m'v_1+(m-m')v_2)^2}{m}\Big)dv_2dv_1dm'\end{aligned} \tag{3.16}$$

The total kinetic energy of particles of mass m may also be decreased by mergers between particles of mass m and any other mass (the second process in the list). Similarly to Eq (3.15), the rate of energy loss may be written

$$\begin{aligned}\dot{E}_\mathrm{loss} = \frac{n(m,t)}{2\pi}\int_0^\infty n(m',t)K(m,m')\int_{-\infty}^{\infty}\frac{1}{\sigma_m\sigma_{m'}}e^{-\left(\frac{v_1}{\sqrt{2}\sigma_m}\right)}\\ \int_{v_1-v_\mathrm{stick}}^{v_1+v_\mathrm{stick}}e^{-\left(\frac{v_2}{\sqrt{2}\sigma_{m'}}\right)^2}\frac{mv_1^2}{2}dv_2dv_1dm'\,.\end{aligned} \tag{3.17}$$

Finally, the total energy of particles with mass m may be decreased by collisions between particles of mass m and particles of any other mass that occur at relative velocities greater than v_stick. In this case, the velocity of both particles is decreased by a factor η relative to the centre of mass. For a collision between particles of masses m_1 and m_2 (velocities v_1 and v_2) the final velocity of particle 1 (denoted v_1') is evaluated by conservation of momentum

$$v_1' = \eta(v_1 - v_\mathrm{com}) + v_\mathrm{com}$$

$$v_\mathrm{com} = \frac{m_1v_1 + m_2v_2}{m_1 + m_2}$$

$$\Delta E = \frac{1}{2} m_1 v_1'^2 - \frac{1}{2} m_1 v_1^2 \,, \tag{3.18}$$

Using these definitions, the change in energy of a particle of mass m_1 by gravitational cooling with a particle of mass m_2, denoted ϵ is given by

$$\epsilon = \frac{m_1}{2}\Big[v_1^2(1-\alpha^2) - v_2^2\beta^2 - v_1 v_2 \alpha\beta\Big], \tag{3.19}$$

where

$$\alpha = \eta + \frac{m_1}{m_1+m_2}(1-\eta) \tag{3.20}$$

$$\beta = \frac{m_2}{m_1+m_2}(1-\eta)\,. \tag{3.21}$$

In a similar way to Eq (3.15) the energy loss via this process may be written

$$\dot{E}_{\rm cool} = \frac{n(m,t)}{2\pi}\int_0^\infty n(m',t)K(m,m') \int_{-\infty}^{\infty} \frac{1}{\sigma_m \sigma_{m'}} e^{-\left(\frac{v_1}{\sqrt{2}\sigma_m}\right)^2} \int^{|v_1-v_2|>v_{\rm stick}} \epsilon e^{-\left(\frac{v_2}{\sqrt{2}\sigma_{m'}}\right)^2} dv_2 dv_1 dm' \,. \tag{3.22}$$

3.2.4 The Solution of the Coagulation Equations

In our simulations we solve the discrete versions of Eq (3.12), Eq (3.8) and Eq (3.9). By assuming that cloud mass is quantised into N bins characterised by an index, i, where $M_i = iM_0$ we can write

$$\dot{n}_k = \frac{1}{2V}\sum_{i+j=k} K_{ij} f_{ij}^m n_i n_j - \frac{n_k}{V}\sum_{j=1}^{j_{max}} K_{jk} f_{ij}^m n_j, \tag{3.23}$$

$$\dot{E}_k = \dot{E}_{\rm gain} - \dot{E}_{\rm loss} - \dot{E}_{\rm cool}, \tag{3.24}$$

$$\dot{\sigma}_k = \frac{\dot{E}_k - \frac{1}{2}\sigma_k^2 M_k \dot{n}_k}{\sigma_k n_k M_k}, \tag{3.25}$$

where subscripts represent different mass bins. $K_{ij} \equiv K(M_i, M_j) \equiv K(iM_0, kM_0)$. The superscript m represents that f is a cross section for particle mergers

To demonstrate the technique for solving these equations we will consider the numerical solution of the simple Smoluchowski equation (Eq (3.10)), which when written in a discrete form takes on the following form

$$\dot{n}_i = \frac{1}{2V}\sum_{j=1}^{i-1} n_j n_{i-j} K_{ij} - \frac{n_i}{V}\sum_{j=1}^{N} n_j K_{ij}. \tag{3.26}$$

Following Benson et al. (2005) Eq (3.26) can be rewritten in the form of a matrix equation

$$\dot{\mathbf{n}} = \mathbf{B} \cdot \mathbf{k}, \tag{3.27}$$

the vector k has $N \times N$ elements corresponding to $K(m_i, m_j)$. The kernel matrix, $\mathbf{B}$ has $N \times N \times N$ elements and may be written more explicitly as

$$\dot{n}_i = \sum_{jk} B_{ijk} k_{jk}, \tag{3.28}$$

where

$$B_{ijk} = \frac{n_j n_k}{V}\Big(\frac{1}{2}\delta_{i,j+k} - \delta_{ik}\Big) \tag{3.29}$$

δ represents a Kronecker delta function. We solve Eq (3.27) implicitly using an iterative method.

The solution of the equations that govern energy exchange between clouds (Eq (3.16), Eq (3.17) and Eq (3.22)) is the same as for the solution of the Smoluchowski equation in that we will write the equations in the form of the linear multiplication of two matrices and then solve this equation implicitly. In order to simplify the notation in this section we will denote the terms in the three equations that are inside of the integrals over velocity as ξ. Explicitly for the case of the equation for energy gain (Eq (3.16)):

$$\begin{aligned}\xi^G(m, m') = \frac{1}{2\pi}\int_{-\infty}^{\infty} \frac{1}{\sigma_m \sigma_{m'}} e^{-\left(\frac{v_1}{\sqrt{2}\sigma_m}\right)^2} \\ \int_{v_1 - v_{\rm stick}}^{v_1 + v_{\rm stick}} \frac{1}{2} e^{-\left(\frac{v_2}{\sqrt{2}\sigma_{m'}}\right)^2} \Big(\frac{(mv_1 + m'v_2)^2}{m}\Big) dv_2 dv_1\end{aligned} \tag{3.30}$$

The corresponding terms in the equations for energy loss(3.17) and cooling (3.22) are denoted $\xi^L(m_1, m_2)$ and $\xi^C(m_1, m_2)$ respectively. Note that the definitions of ξ include the factors of 2π and $\frac{1}{\sigma}$ from throughout the equations.

The equation for the total evolution of the energy of a system of coagulating and cooling particles may be written in terms of these new functions as:

$$\begin{aligned}\dot{E}(m) = &\int_0^{\infty} n(m', t) n(m - m', t) K(m', m - m') \xi^G(m', m - m') dm' \\ &- n(m, t) \int_0^{\infty} n(m', t) K(m, m') \xi^L(m, m') dm' \\ &- n(m, t) \int_0^{\infty} n(m', t) K(m, m') \xi^C(m, m') dm'\end{aligned} \tag{3.31}$$

Which when discretized and rearranged becomes

$$\dot{E}_i = \sum_{j=1}^{i-1} n_i n_j K_{ij} \xi_{ij}^G - n_i \Big(\sum_{j=1}^{N} n_j K_{ij} \big(\xi_{ij}^C + \xi_{ij}^L\big)\Big) \tag{3.32}$$

The subscripts represent different mass bins ($n_j \equiv n(jM_0)$). Our goal is to rewrite Eq (3.32) in the form of a linear multiplication of two matrices

$$\dot{\mathbf{E}} = \mathbf{C} \cdot \mathbf{k}, \tag{3.33}$$

where $\mathbf{k}$ is defined in the same way in the solution of the Smoluchowski equation, that is: $k_{ij} \equiv K(m_i, m_j)$. The form of $\mathbf{C}_{ijk}$ that is consistent with Eq (3.32) is given by:

$$C_{ijk} = n_j n_k \Big(\delta_{i,j+k} \xi^G_{jk} - \delta_{ik} \big(\xi^C_{jk} + \xi^L_{jk} \big) \Big) \tag{3.34}$$

This form for $\mathbf{C}_{ijk}$ is functionally equivalent to $\mathbf{B}_{ijk}$ (Eq (3.29)) so the solution may proceed in exactly the same way as for the Smoluchowski equation, the only difference is the form of the matrix $\mathbf{B}$

The calculation of the quantities ξ^G, ξ^C and ξ^L is computationally very expensive so they are initialised once into a lookup table at the start of every simulation and obtained by bilinear interpolation thereafter

3.2.5 Cloud Collapse and Star Formation

The vast majority of stars form in Giant Molecular Clouds. This process is described in the sticky particle model by allowing the most massive clouds in the galaxy to collapse into stars.

Relevant Physics

We follow the process of star formation in our simulations by waiting for star forming clouds to be created by the coagulation process described in section 3.2.2. We define star forming clouds to be clouds of a mass similar to the most massive clouds observed in the MW ($\sim 10^6 M_\odot$). When one of these star forming clouds is created it is assumed to collapse on a short timescale and approximately $\epsilon_\star \sim 10\%$ of its mass is converted into stars, whilst the remainder is disrupted by stellar feedback processes including stellar winds, SN feedback and photoionization. This process reflects that although stars may form in less massive molecular clouds, it is not until the relatively rare, massive O and B stars are created that the cloud is destroyed (Elmegreen (1983)).

We assume that each cloud collapse forms a single stellar population with an IMF of the standard Salpeter (1955) form

$$N(M)\, dM \propto M^{-(1+x)} dM\,, \tag{3.35}$$

where x is the slope of the IMF and takes the usual value of 1.35. The masses of stars are assumed to lie between well defined minimum and maximum values, $M_{\star,\min}$ and $M_{\star,\max}$.

Numerical Implementation

The treatment of star formation adopted in most simulations is to identify gas that is likely to be star-forming and impose a star formation rate given by the Schmidt law,

$$\dot{\rho}_\star = C\rho_{\rm gas}^{N_{\rm SF}} \, . \tag{3.36}$$

Here, $\dot{\rho}_\star$ and $\rho_{\rm gas}$ denote the rate of star formation per unit volume and the gas density respectively. This power law relation between star formation rate (SFR) and gas density was found to hold over many orders of magnitude by Kennicutt (1988), who constrained the exponent to be $N_{\rm SF} = 1.4 \pm 0.2$.

We take a different approach: unstable molecular clouds are identified in the simulations as any cloud with a mass greater than $M_{\rm sf}$. We identify the formation of these massive clouds by using the cloud mass function, as stored internally to every single sticky particle. These unstable clouds are assumed to collapse on a very short timescale, forming stars.

As soon as a cloud of mass $M_{\rm sf}$ forms, it is assumed to be disrupted by OB stars on a timescale of $\sim$10Myr (Matzner (2002)), the rest of the massive cloud is broken down into smaller clouds and the coagulation process begins all over again as described in section 3.2.2. This process is modelled by taking the fraction of the cloud's mass that does not turn into stars, $1-\epsilon_*$, and assuming that the net effect of the stellar feedback processes is to fragment the GMC into the smallest clouds represented in the sticky particle internal mass function. This has the net effect of steepening the cloud mass function.

Each star particle formation event represents the formation of a single stellar population of stars that are all assumed to have the same age, and to be drawn from the Salpeter IMF. Each stellar particle is therefore formed with a mass approximately equal to ϵ_* times the mass of a starforming cloud. If this particle mass is not allowed by the mass resolution of a given simulation then we either store up unresolved stars internal to a sticky particle (if the star mass is too small to be allowed), or split it into multiple, equal mass particles (if the star mass is too large to be allowed).

3.2.6 Supernova Feedback

Our simulations include only energy feedback from type II SN. These events return energy from the stars to the ambient phase. We note that it is not currently computationally feasible to resolve the properties of SN remnants so we treat them with a simple, analytic prescription. The mechanism by which SN feedback is implemented in our model is discussed here.

Relevant Physics

Each star of mass greater than $8M_\odot$ releases $10^{51}E_{51}$ ergs in thermal energy when it undergoes a SN event. The lifetime, t, of a star of mass M (where $M > 6.6M_\odot$) is given by (Padovani and Matteucci (1993))

$$\frac{t}{\mathrm{Gyr}} = 1.2\left(\frac{M}{M_\odot}\right)^{-1.85} + 0.003\,. \tag{3.37}$$

Each SN explosion can be approximated as the injection of energy at a single point in space. If we assume that the ambient density on scales of interest is approximately homogeneous, with density ρ_h, then each SN explosion can be modelled as a Sedov blast wave (Sedov (1959)). According to this solution, if at time $t = 0$ we release an amount of energy E_b, then after time t the resulting blast wave will have reached a radius r_b given by

$$\begin{aligned} r_b &= \left(\frac{E_b}{\rho_h}\right)^{1/5} t^{2/5} \\ &= 292\left(\frac{E_b/10^{51}\mathrm{ergs}}{\rho_h/0.1\,\mathrm{cm}^{-3}}\right)^{1/5} (t/10\mathrm{Myr})^{2/5}\,\mathrm{pc}\,. \end{aligned} \tag{3.38}$$

These hot SN bubbles have two main effects. Firstly, as they expand and decelerate the SN heated gas will get mixed in with the surrounding ambient medium; the net result of this process is the heating of the ambient medium. Secondly, as discussed in section 3.2.7, any cold clouds caught inside a SN bubble will undergo evaporation.

There are two main assumptions that must hold for the Sedov solution to be valid, the pressure of the ambient medium, and the cooling rate inside the bubble, must both be negligible. Often at least one these assumptions is invalid. If the ambient medium has a low density and is very hot, for example due to a previous set of explosions, then its pressure is no longer negligible and the Sedov solution breaks down. If the ambient medium is dense then radiative cooling becomes an important process. In the remainder of this section we describe various modifications to the standard Sedov solutions, which allow us to model SN remnants in a wider variety of conditions.

In the case of a hot, tenuous medium the radius of each blast wave is increased (Tang and Wang (2005)). These authors derive a fitting formula for the velocity of a SN blast in a hot medium, which is accurate to within 3%

$$r_b(t) = \int_0^t c_h \Big(\frac{t_c}{t'} + 1\Big)^{3/5} dt' \,, \tag{3.39}$$

$$= 156 \int_0^{t/\mathrm{Myr}} \Big(\frac{t_c}{t'} + 1\Big)^{3/5} dt' \ \mathrm{pc}, \tag{3.40}$$

where c_h is the sound speed of the ambient medium. We assumed a temperature of $T_h = 10^6$K, mean molecular weight of $\mu = 0.58$, blast wave energy of 1×10^{51} ergs and an ambient density of 0.1 atoms per cm^3 in order to illustrate the order of magnitude of r_b. t_c is a characteristic time,

$$\begin{aligned} t_c &= \left[\Big(\frac{2}{5}\xi\Big)^5 \frac{E_b}{\rho_h c_h^5}\right]^{1/3} \\ &= 0.012 \left[(\xi/1.14)^5 \, \frac{E_b/10^{51}\mathrm{erg}}{(\rho_h/0.1\,\mathrm{cm}^{-3})(T_h/10^6\mathrm{K})^{5/2}}\right]^{1/3} \mathrm{Myr}\,. \end{aligned} \tag{3.41}$$

where ξ equals 1.14 for a gas with adiabatic index $\gamma = 5/3$. This solution matches the standard Sedov evolution, $r_b \propto t^{2/5}$, closely until $t \sim t_c$, after which the shell's velocity becomes constant, $r_b \propto t$. This modification allows us to take into account that the majority (∼90%) of SNII happen in preheated SN bubbles (Higdon et al. (1998)) and, therefore, the approximation that the pressure of the ambient medium is negligible is often incorrect. Fig (3.3) shows the difference between an adiabatic gas SPH simulation of a SN induced shock-wave, the pure Sedov solution and the blast wave radius as predicted by the hot medium-modified Sedov solution from Tang & Wang (2005).

Situations where radiative cooling are important may be taken into account using the prescription of Thornton et al. (1998), whose high resolution simulations of SN explosions expanding in an ambient medium with temperature $T_h = 10^3$K, provide the total thermal energy in SN bubbles as a function of time, ambient density and metallicity. We perform bilinear interpolation on the results in tables 2 and 4 of Thornton et al. (1998) to obtain the SN bubble radius and thermal energy at any given time.

Neither of these solutions treats the more general case of SN remnant expansion in a porous ISM, which may have regions of both high and low ambient density, and so we are not able to include the effects of SNe in a fully self-consistent manner. In most of our simulations we use the simple Sedov solution for the evolution of the SN blast waves, but

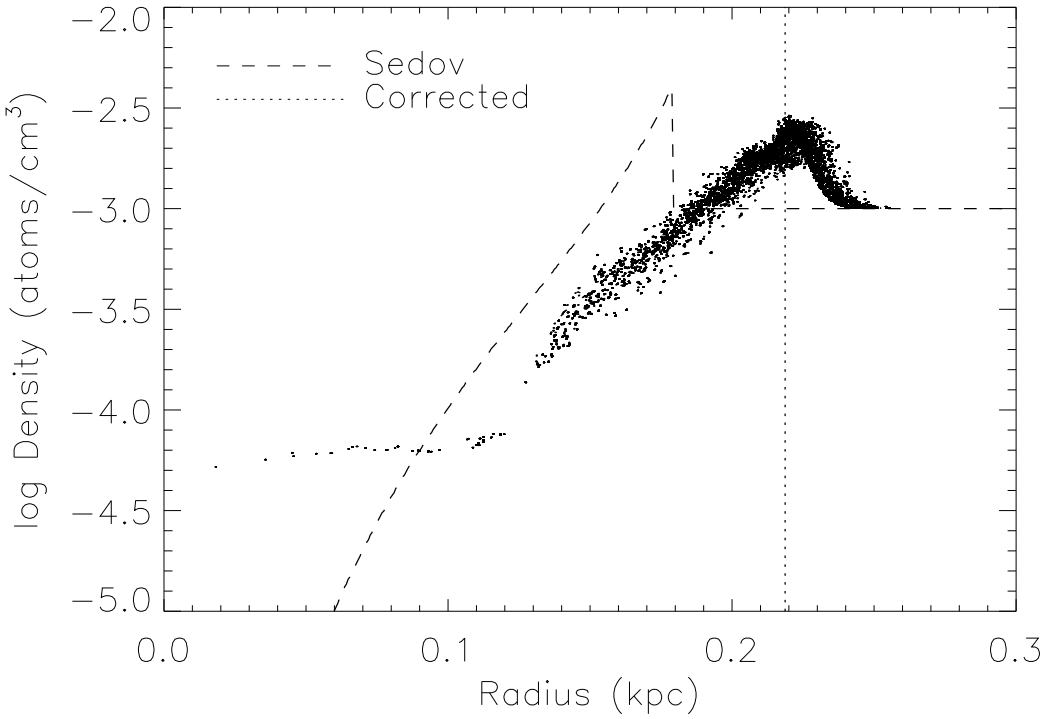

Figure 3.3: Comparison between SPH simulation of a Sedov blast, the Sedov solution and the hot medium correction of Tang & Wang (2005). The points represent individual SPH particles, the dashed line is the Sedov solution and the dotted line is the blast wave radius as calculated with the hot medium correction. The initial condition had a density of 0.001 atoms per cm^3 and a temperature of 10^6K. 10^{51}ergs were injected to the central 32 particles at t_0. This plot was made after the blast wave had evolved for 0.3 Myr.

note that the details of our prescription are uncertain. In section 4.4 we investigate the effects of using different implementations of the physics of SN blast waves to estimate how important the details of the behaviour of SN remnants are to the overall properties of the galaxy. Both the radiative cooling and blast wave velocity physics are varied.

Numerical Implementation

By assuming that each stellar particle in the simulation represents an entire population with the same age we can calculate the minimum and maximum masses of stars that undergo supernova events over any given time period using Eq (3.37). Each of these supernovae is assumed to go off in a neighbouring gas particle (*i.e.* one for which the distance, r, to the star is smaller than its smoothing length, h, in the SPH formalism). We chose this particle randomly from the neighbours, with a weight computed from the solid angle, Ω, it subtends on the sky as seen from the position of the star particle,

$$\Omega = 2\pi \left(1 - \frac{r}{\sqrt{(r^2 + h^2)}}\right). \tag{3.42}$$

This weighting forces that nearby hot, diffuse gas (which tends to have larger h, hence larger weight) is heated more frequently than cooler, denser parts of the ambient medium (which are dense, hence have smaller h).

We do not transfer all SN energy to gas particles each timestep. Assuming that SN explosions are distributed evenly in time and space we can calculate for every ambient gas particle a 'porosity' of SN bubbles, $Q = V_{\rm B}/V_{\rm A}$. For the volume associated with a gas particle we use $V_{\rm A} = (4\pi/3)\, h^3$, and $V_{\rm B} = (4\pi/3) \sum r_b^3$ is the total volume of all the SN bubbles in this particle. When Q is greater than a critical value, $Q_{\rm crit} \approx 1$, the ambient phase is heated, else the available SN energy is carried over to the next time step. This ensures that the ambient phase is only heated when hot supernova bubbles make up a significant fraction of the volume. There are two motivations for this, firstly a given SPH particle cannot represent more than one phase at a given time. Secondly simulations usually do not limit the timestep to be a fraction of the cooling time. Consider a warm, $T \sim 10^4$K, SPH particle in the disk. If a small amount of SN energy is injected into this dense particle, it will cool very efficiently since the cooling rate is very high. It is only when the particle is heated to $T \gg 10^6$K that the reduced cooling may affect the particle dynamically, so that it will move into lower density gas, further decreasing its cooling rate, and becoming part of the hot, tenuous gas. Storing the available heating until the SN bubbles fill a significant fraction of the particle is a way of easing the transition from

warm to hot and makes the outcome less dependent on the timestep.

To determine the porosity Q, we need to know the current radii, r_b, of SN bubbles. The radius r_b depends on the ambient gas properties and also on the available energy, E_b, as discussed in section 3.2.6. Typically a single stellar particle will undergo multiple SN events over a single timestep. Using Eqs. (3.37) and (3.38) and obtaining the SPH estimate of the ambient gas density at the position of the star particle we can estimate the average radius of all supernova bubbles blown by a given star particle at any time. Working under the assumption that the porosity of the ISM is low we calculate the radiative loss from each bubble separately. When the porosity of the ISM becomes $Q > Q_{\rm crit} \sim 1$, the SN bubbles are overlapping significantly and all coherent structure is assumed to be wiped out. The ambient gas particles are heated by the remaining thermal energy in the supernova bubbles and they are considered to disperse. The porosity is set back to zero. Note that using the Sedov solution implies we neglect radiative cooling in the remnants to determine the porosity, Q. However to determine how much energy is in the bubbles once we decide to heat the particle, we do use the tables of Thornton et al. (1998) to account for radiative cooling in the SN shells. We believe that even though this treatment is not fully consistent, it does capture the main physics.

3.2.7 Thermal Conduction

Thermal conduction between the ambient and cold gas in the simulation is an important ingredient in the self-regulation of the star formation rate in our model of the ISM.

Relevant Physics

Thermal conduction has two primary effects. The first is to smooth out the temperature and density profiles inside SN remnants. In the strong explosion solution of Sedov, where thermal conduction is neglected, the temperature of the blast wave increases sharply towards the centre of the blast. This is due to the fact that the gas near the origin was heated by a stronger shock than that at the edges and thereafter evolves adiabatically. The effect of thermal conduction is to efficiently transport heat from the centre of the blast to the outer cool regions. The temperature of the interior of the supernova blast, T_b, is then approximately constant and equal to the mean temperature of the blast(Chevalier (1975); MO77):

$$\left(\frac{T_b}{10^8\mathrm{K}}\right) = 1.2\left(\frac{r_b}{10\mathrm{pc}}\right)^{-3}\left(\frac{n_b}{0.1\,\mathrm{cm}^{-3}}\right)^{-1}\left(\frac{E_b}{10^{51}\mathrm{erg}}\right), \tag{3.43}$$

where n_b and T_b are the mean density and temperature inside the bubble, respectively. We assume r_b to be described by Sedov's self-similar solution. The density n_b is also approximately constant and is given in terms of the ambient density, n_h, as

$$\frac{n_b}{n_h} = 1 + x^{-5/3} \tag{3.44}$$

$$x \equiv 0.65 \Big(\frac{r_b}{10\mathrm{pc}}\Big) \Sigma_{\mathrm{con}}^{1/5} (\frac{n_h}{\mathrm{cm}^{-3}})^{3/5} (\frac{E_b}{10^{51}\mathrm{erg}})^{-2/5} . \tag{3.45}$$

The dimensionless number Σ_{con} represents the effectiveness of evaporation,

$$\Sigma_{\mathrm{con}} = \frac{\alpha_{\mathrm{con}}}{3} \Big(\frac{r_c}{\mathrm{pc}}\Big)^2 f_{\mathrm{cl}}^{-1} \phi^{-1}, \tag{3.46}$$

(McKee and Cowie (1977)), and depends on $\alpha_{\mathrm{con}} = \dot{r}_b / c_h$ (the ratio of the velocity of the supernova blast wave to the sound speed of the medium), the cloud's radius, r_c, the volume filling factor of the cold clouds, f_{cl}, and the efficiency of thermal conduction, ϕ (see MO77 for details). For a pure Sedov blast wave $\alpha_{\mathrm{con}} = 1.68$. The presence of magnetic fields and turbulence may decrease ϕ below its maximum value of $\phi = 1$. We compute f_{cl} for each sticky particle from its current cloud mass spectrum given the assumed cloud mass-radius relation, Eq. (3.5).

The second effect of thermal conduction is to evaporate cold clouds. According to (McKee and Cowie (1977); Cowie (1977)), the evaporation rate is well described by:

$$\Big(\frac{\dot{M}_c}{\mathrm{M}_\odot \mathrm{Myr}^{-1}}\Big) = -0.44 \times \Big(\frac{T}{10^6 \mathrm{K}}\Big)^{5/2} \Big(\frac{r_c}{\mathrm{pc}}\Big) . \tag{3.47}$$

Numerical Implementation

Since we store the mass function of molecular clouds internal to each sticky particle explicitly (Sect. 3.2.2), we can apply Eq. (3.47) along with Eq. (3.5) to each cloud mass bin to calculate the total mass loss of a cloud over one timestep. The evaporation rate of the cloud depends on the temperature of the ambient gas, which is represented with SPH particles. However, as we discussed above, some fraction Q of the volume of each SPH particle may be filled by hot SN bubbles, in which the evaporation rate of clouds may be much higher. Since we have computed Q, we can take this important effect into account.

Consider a single molecular cloud in thermal contact with an ambient medium of (constant) temperature T. The mass of a cloud at the end of a timestep (M_f) is related to its mass at the start of the timestep (M_i) by:

$$M_f = \Big[M_i^{1-\alpha_c} - (1-\alpha_c) \frac{0.44 T^{5/2} r_{\mathrm{ref}}}{M_{\mathrm{ref}}^{\alpha_c}} \Delta t \Big]^{1/(1-\alpha_c)} , \tag{3.48}$$

where T is in units of 10^6K, masses are in $M_\odot$, lengths are in pc and times are in Myr.

Eq (3.48) represents the mass loss rate for a single cloud in contact with a medium of temperature T. More generally in a porous medium a single cloud of mass m has a mean mass loss rate described by:

$$\dot{M}_{\rm cloud} = -Q\dot{M}_{\rm bubble} - (1-Q)\dot{M}_{\rm ambient}, \tag{3.49}$$

where $\dot{m}_{\rm bubble}$ and $\dot{m}_{\rm ambient}$ represent the rate of mass loss for a cloud inside a supernova bubble and situated in the ambient medium respectively.

Eq. (3.48) can be applied directly to the evaporation of a cloud in the local ambient medium ($\dot{m}_{\rm ambient}$). However to apply the same formula to the evaporation of clouds inside of supernova bubbles we need to account for the fact that although the temperature inside the bubbles remains uniform, due to conduction, it is not constant in time, but decreases as the bubble expands. We therefore make the additional assumption that the mean temperature of the supernova remnant is constant over a timestep (a good approximation after a short transient phase). Under this assumption Eq. (3.48) can be applied successfully to the more general case of evaporation in a porous medium. Eq (3.47) and Eq (3.5) are used to show that the total mass loss rate for clouds of mass m in a volume V_A is given by

$$\Big(\frac{\dot{M}}{\rm M_\odot Myr^{-1}}\Big) = -0.44\Big(\frac{M_c}{M_\odot}\Big)_c^{\alpha}\Big(\frac{r_{ref}}{\rm pc}\Big)\Big(\frac{M_{ref}}{\rm M_\odot}\Big)^{-\alpha_c}\left(Q\Big(\frac{T_b}{10^6{\rm K}}\Big)^{5/2} + (1-Q)\Big(\frac{T_a}{10^6{\rm K}}\Big)^{5/2}\right). \tag{3.50}$$

Under the assumption that T_b, the mean temperature of supernova remnants, and T_a, the mean ambient temperature, are constant over any single timestep we can write

$$\Big(\frac{\dot{M}}{\rm M_\odot Myr^{-1}}\Big) \equiv \lambda\Big(\frac{M}{M_\odot}\Big)^{\alpha_c}, \tag{3.51}$$

In order to calculate the constant of proportionality, λ, we use an estimate of the mean temperature and density inside of a supernova remnant. These estimates were obtained by noting that by definition $Q \equiv V_B/V_A$. (V_B and V_A represent the total volume in bubbles and the ambient phase respectively). The mean radius of a supernova remnant is then

$$r_b = \Big(\frac{3QV_A}{4\pi N_{SN}}\Big)^{1/3}, \tag{3.52}$$

where N_{SN} is the total number of supernova explosions that have affected the local ambient medium (calculated from equations 3.37 and 3.35). The mean density inside the

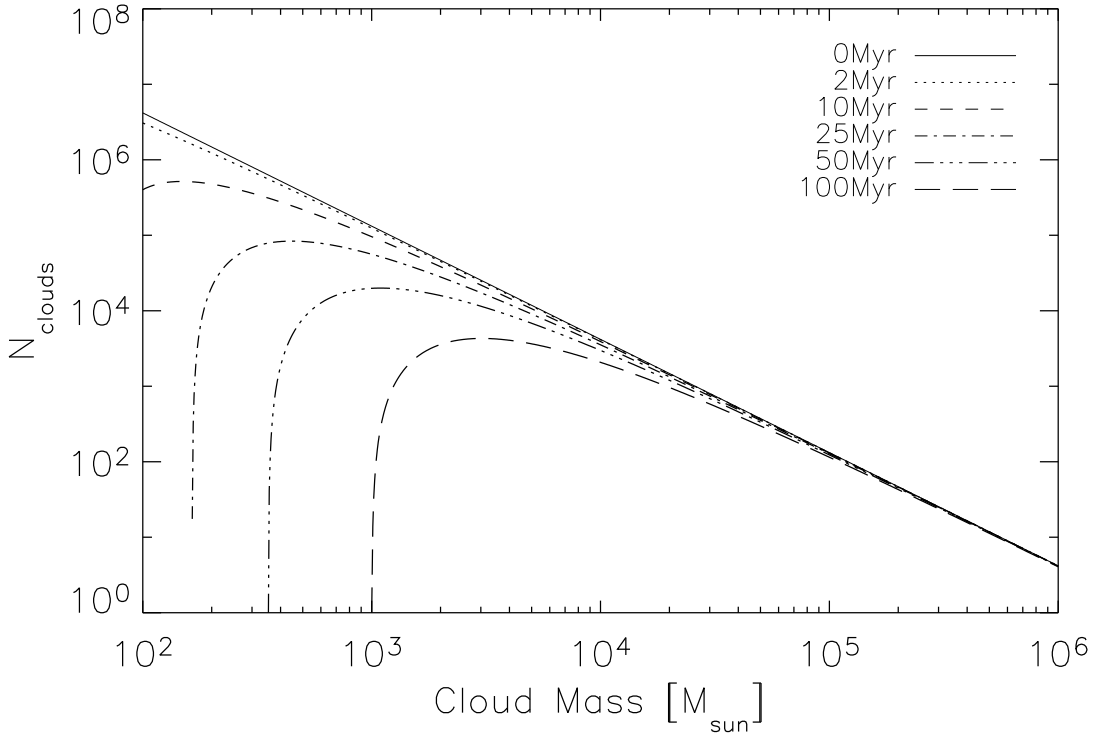

Figure 3.4: Evolution of a population of molecular clouds as they are evaporated by a hot ambient medium. The initial cloud mass function is a power law. The temperature of the ambient medium is assumed to be 10^5K, the porosity of the medium is assumed to remain constant at 0.2, and the temperature of the supernova remnants is $\approx 10^6$K. Thermal conduction acts to preferentially destroy the smaller clouds.

supernova remnants, n_b, may then be calculated from Eq (3.44) and Eq (3.45) and the mean temperature from Eq (3.43).

Over a period of time Δt a cloud with mass M_I will evaporate to a mass of M_F, given by:

$$M_F = \left(M_I^{(1-\alpha_c)} - \lambda \Delta t \right)^{1/(1-\alpha_c)} \tag{3.53}$$

Thermal conduction efficiently destroys smaller clouds, but its effects are far less dramatic on larger clouds. Fig (3.4) shows the evolution of an initially power law mass spectrum of clouds in a hot medium. The energy used to evaporate a mass $M_F - M_I$ of cold clouds is removed from the supernova remnants.

3.2.8 Mass Resolution Limits

The sticky particle model allows particles of all types to change their mass via processes including merging, thermal conduction and star formation. For this reason it is necessary for us to introduce numerical minimum and maximum masses on all particle types. We define at the initial time a characteristic mass resolution for our simulation, $M_{\rm char}$, typically this is set equal to the mass of the ambient gas particles in the initial conditions. Where more than one mass of ambient particles is present (for example in the model galaxies discussed in section 4.1) we use the mass of the gas particles that will be forming most stars. We then define minimum and maximum particle masses relative to this characteristic mass scale.

Ambient gas particles may have their mass decreased by the formation of molecular clouds. If the total mass of a gas particle becomes less than $0.1M_{\rm char}$ then it is converted entirely into a cloud particle. The ambient gas particles may also have their mass increased by the process of thermal conduction. If a gas particle becomes more massive than $4M_{\rm char}$ then it is not allowed to grow any more, and the evaporated cloud mass is given to a different particle. In practice this limit is rarely, if ever, reached as evaporating cold clouds effectively cools the ambient gas particles so they become inefficient at thermal conduction.

Sticky particles may decrease their mass by star formation and evaporation. If the mass of a sticky particle drops below $0.1M_{\rm char}$ then it is either completely evaporated or completely converted into stars. Coagulation may drive the mass of a sticky particle to be very large. In practice this is not a real concern since when a sticky particle becomes very massive the rate at which its internal clouds coagulate also increases, causing it to form stars very rapidly.

Stars have a maximum and minimum mass of $4M_{\rm char}$ and $0.1M_{\rm char}$. If a star forms with a mass greater than the maximum allowed mass it is split into a number of smaller star particles. A sticky particle may not form a star with a mass lower than the minimum allowed mass. In this eventuality then the mass of the 'unresolved' stars is tracked internally by the sticky particle and added into the next star formation event until the total mass of stars formed reaches the resolution limit of the simulation.

These particle mass limits keep all particle masses in the range $0.1M_{\rm char}$ to $4M_{\rm char}$, which both minimises two body effects between very massive and very small particles and also prevents the formation of very many low mass particles, which are computa-

tionally very expensive to evolve.

3.3 Parameter Estimation

The various physical processes in the star formation and feedback models each have associated with them physical parameters. Before we discuss the properties of our model in detail we discuss how its free parameters can be constrained.

The free parameters that control the thermal instability and formation of the molecular clouds are $\rho_{\rm th}$ and $T_{\rm th}$, the physical density and temperature at which thermal instability is allowed to set in and radiative cooling creates molecular clouds. Wolfire et al. (1995) found that a diffuse ISM naturally settles into two stable phases, with a sharp cutoff between the ambient and molecular phases at a density of approximately 1 atom per cm^3. We use this as the value of $\rho_{\rm th}$. A threshold temperature $T_{\rm th} = 10^5$K allows the gas in galaxies which cools radiatively to $\sim 10^4 K$ to collapse into clouds but prevents supernova heated material (typically at temperatures of $10^6 K$) from forming molecular clouds until it has radiated away most of its supernova energy.

The properties of the molecular clouds themselves are contained in four parameters: $r_{\rm ref}$, $M_{\rm ref}$, and α_c as defined in Eq (3.5) and u_c, the internal energy per unit mass of molecular clouds. The first three values are set by comparison with observations of molecular clouds in the nearby galaxy M33 (Wilson and Scoville (1990)):

$$\Big(\frac{r_{\rm c}}{\rm pc}\Big) = (36 \pm 6)\Big(\frac{M}{10^5 M_\odot}\Big)^{0.3\pm0.1} \tag{3.54}$$

Thus $r_{\rm ref}$ and $M_{\rm ref}$ are assumed to be 36pc and $10^5 M_\odot$ respectively. This calibration (and an assumed α_c of 0.3) suggest a radius of 122 ± 6pc for the largest clouds observed in the MW ($6 \times 10^6 M_\odot$ (Williams and McKee (1997)).

The properties of the stars and associated feedback are contained within four parameters: x, the slope of the IMF; E_{51}, the energy of each supernova blast in units of 10^{51}erg; $M_{\star,\rm min}$, the minimum star mass; and $M_{\star,\rm max}$, the mass of the largest allowed stars. For E_{51} we use the fiducial value of 1.0 noting, however, that the value of E_{51} is very uncertain and may be significantly higher. The effects of varying E_{51} are investigated in section 4.4. For the purposes of this work uncertainties in the IMF are neglected and x is assumed to take on the standard Salpeter value of 1.35. We follow Kawata and Gibson (2003) in adopting values $0.2 M_\odot$ and $60 M_\odot$ for the minimum and maximum stellar masses, respectively.

The star formation efficiency in a single cloud collapse is also somewhat uncertain and is known to be approximately $\epsilon_\star \approx 11\%$ (Williams and McKee (1997)) in the MW.

The thermal conduction efficiency is characterised by two numbers: $\alpha_{\rm con}$, the ratio of the blast wave velocity to the ambient sound speed and ϕ, the efficiency of thermal conduction. Following MO77, the value of $\alpha_{\rm con}$ is set to 2.5 (for the ideal Sedov blast wave case, $\alpha_{\rm con}$ is 1.68, the presence of thermal conduction changes this value). The thermal conduction efficiency parameter is assumed to be $\phi = 1$. The presence of magnetic fields and turbulence may change ϕ significantly; we investigate the effect of moving away from this value in Sect. 4.4

This leaves $v_{\rm stick}$ (the maximum relative cloud velocity for mergers) and η (the fraction of a cloud's velocity lost per non-merger collision) as free parameters that are hard to constrain via observation. It is noted that the large scale behaviour of a given simulation is largely independent of the value of η. This is because the cold cloud velocity dispersion is always limited by $v_{\rm stick}$. In the following section simple simulations are used in order to calibrate the properties of the physical model.

3.3.1 One Zone Simulations

Simulation Details

A 'one zone model' is a periodic box that represents a fixed mass and volume (i.e. a static, periodic box with no mass outflow). The ambient ISM phase is assumed to be homogeneous. Initially, for a chosen mean density of matter we assume that 50% of the material is initially in the hot phase at a temperature of $T_0 = 10^6$K. The remaining gas is initially in cold clouds with an initial mass function that is a very steep ($N(M)dM \propto M^{-8}dM$) power law. Numerically we represent the different phases as follows: the ambient phase is assumed to be homogeneous and isotropic and so is represented by a single density and temperature throughout the whole periodic volume, molecular clouds are represented by discrete sticky particles that are spawned at a random point in the computational volume with a random velocity, stars are not tracked individually, and are assumed to heat the whole volume evenly when they undergo SN explosions. The mass resolution of the molecular phase is approximately $10^7 M_\odot$, although the effects of varying this figure are investigated later in this section.

This initial situation represents hot, dense gas that has just begun to experience a thermal instability and started forming its first molecular clouds. The volume we sim-

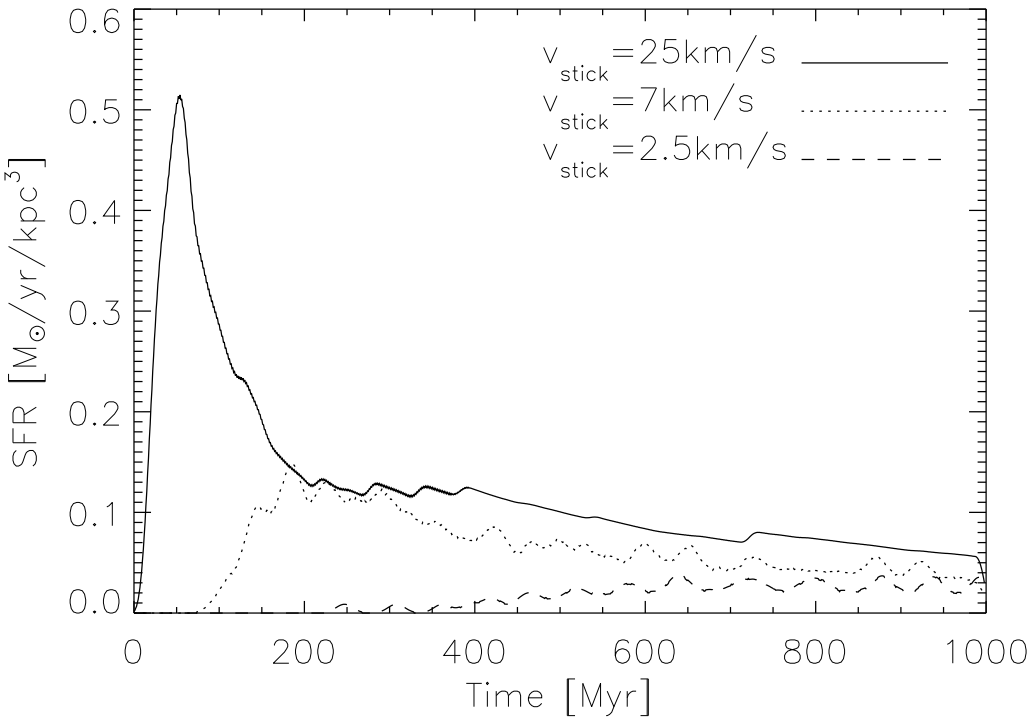

Figure 3.5: Star formation rate as a function of time for a one zone box with three different values of $v_{\rm stick}$. The initial gas density is $n_0 = 2$ cm^{-3} in each case. Each curve follows the same general shape, there is an initial delay during which the first GMCs are forming. The unopposed collapse of the first GMCs causes a burst of star formation, which is quickly regulated by the effects of feedback from stellar winds and supernova explosions. After this initial burst the star formation rate in the simulation settles down and gradually decreases as the gas in the box is used up.

ulate is one cubic kpc. The hot phase will evaporate cold clouds through thermal conduction, and can cool via radiative processes using a simple tabulated cooling function from Sutherland and Dopita (1993) (assuming solar metallicity). Cold cloud particles are scattered randomly throughout the volume and given random velocities. Clouds do not feel gravitational forces. Depending on the parameters, the ambient phase will cool radiatively to form more molecular gas. Clouds will coagulate to form GMCs, which in turn form stars. The associated SNe evaporate smaller clouds, and may heat the ambient medium and quench the star formation. This sequence of events is plotted in Fig (3.5), the same general shape is observed for each value of $v_{\rm stick}$, there is a brief delay as the first clouds coagulate to form GMCs, these clouds then collapse and form stars, which undergo supernovae and quench the star formation. On a longer timescale, the quiescent star formation rate slowly decreases as the available gas is consumed by stars. Since the dynamical equilibrium is reached on a very short timescale, typically a couple of hundred Myr, we assume instantaneous recycling when considering supernova feedback. The role of T_{th} is suppressed in the one zone simulations, due to the fact that energy injected via supernovae cannot escape the volume.

The lack of self gravity does not affect the global properties of the volume significantly. From Eq (3.7) assuming typical cloud properties ($M_c \approx 10^5 M_\odot$, $r \approx 50{\rm pc}$) and a reasonable velocity dispersion ($\sigma = 7{\rm km/s}$) the ratio of the geometric part of the cross section to the gravitationally focused part is approximately 0.1, therefore direct collisions between clouds account for the majority of the collisions and gravitational focusing makes for an effect of only 10%. In the following section we will choose a value of $v_{\rm stick}$ by comparing the star formation rates in one zone volumes with the Schmidt law, and also look at the properties of one zone volumes.

As noted in section 3.3 the properties of the simulation are largely independent of η. We assume a value of 0.5 throughout the rest of this thesis.

Calibrating the base model

The one zone model provides a useful sandbox in which we can investigate a wide variety of parameter choices in a relatively computationally inexpensive environment. In the following section we discuss our choices for the values of the different parameters. The effects of moving away from this 'base model' are discussed more fully in later sections.

The parameters that are available for tuning the output of the model are as follows: the cold cloud reference size and radius ($r_{\rm ref}$, $M_{\rm ref}$); the slope of the cloud mass-radius

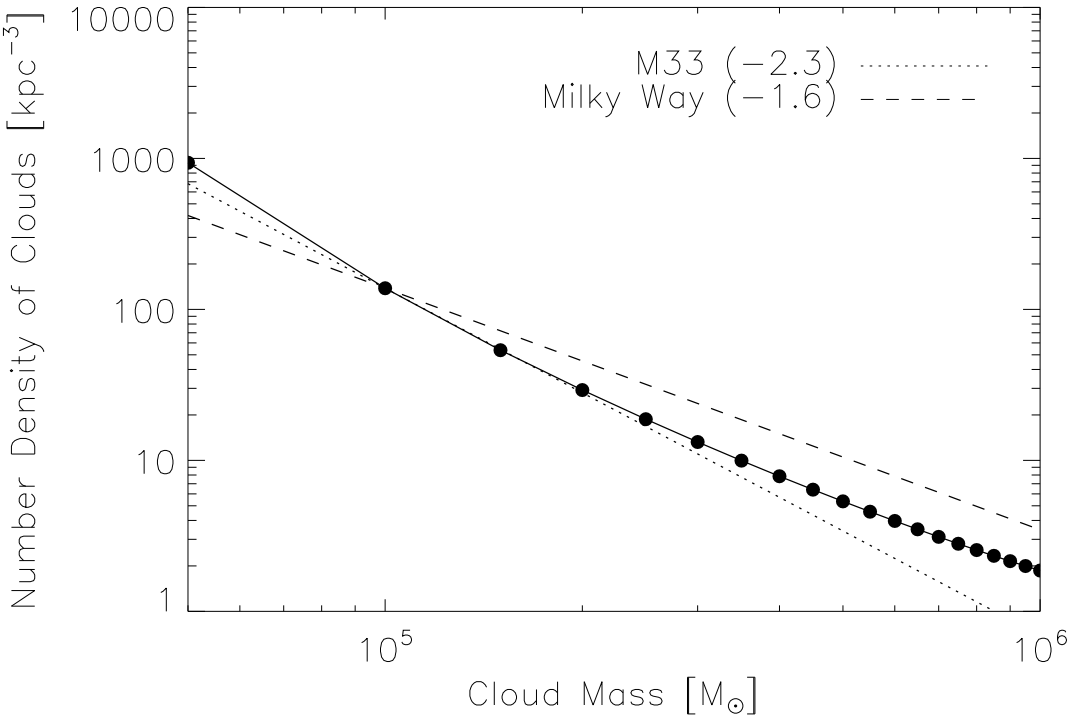

Figure 3.6: Mass function of clouds after 1Gyr in a one zone model. The dashed and dotted lines represent the slopes of the mass functions in the MW (Solomon et al (1987))and M33 (Rosolowsky & Blitz (2004)). The numbers in the legend represent the power law slopes in each of the galaxies. It is clear that we obtain a good agreement between our model and the cloud mass spectrum in real galaxies.

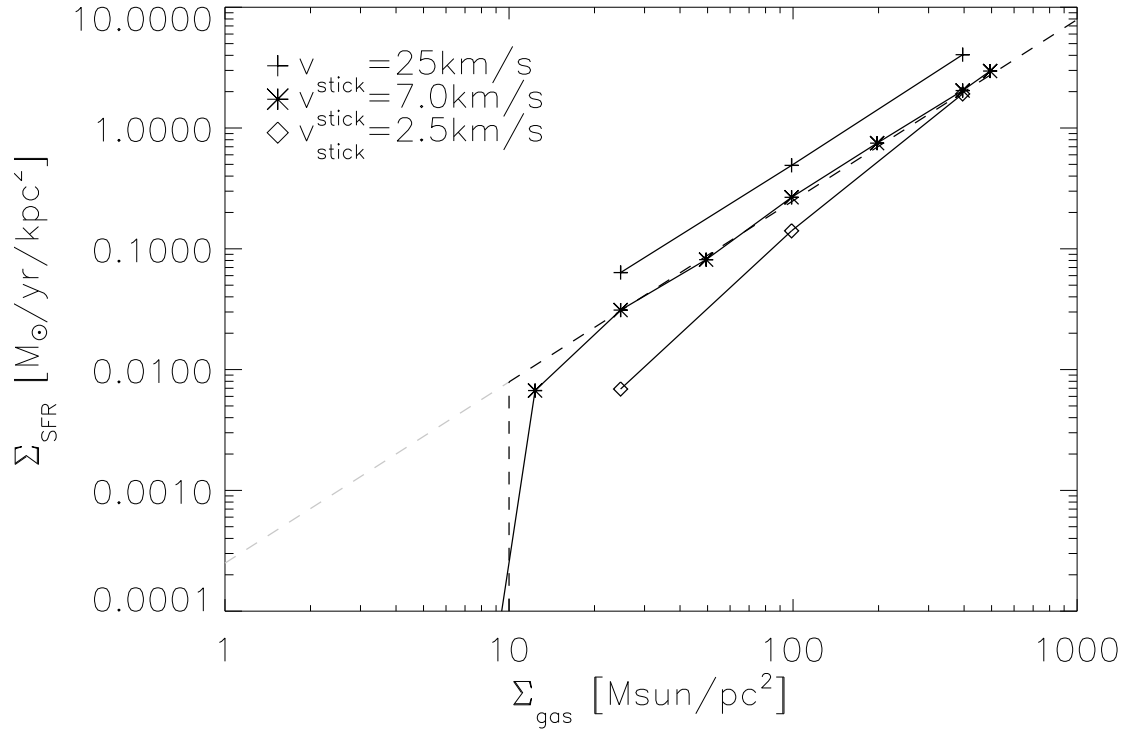

Figure 3.7: Schmidt law. The diagonal dashed line represents the observed star formation law (Kennicutt 1998) and the vertical line represents the observed cutoff in star formation ($10 M_\odot \mathrm{pc}^{-2}$; Schaye 2004). Each point represents the star formation rate averaged over a period of 500Myr for a separate one zone simulation. Data is shown for two different values of v_{stick}, the base value used in all subsequent simulations is 7km/s. We calculate star formation rates by averaging the star formation rate in the simulation volume over a 500Myr period. Surface densities were calculated from volume densities by assuming a disk of thickness of 1kpc.

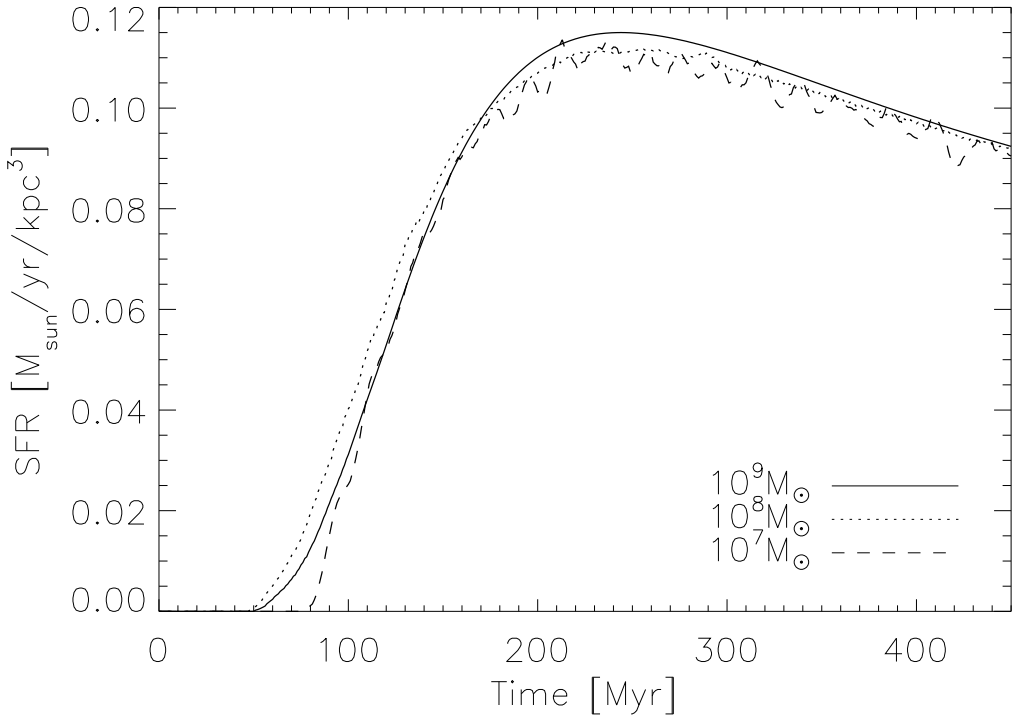

Figure 3.8: Star formation rate as a function of time for one zone models with three different mass resolutions. The star formation rate remains almost unchanged over two orders of magnitude in mass resolution. The coarsest mass resolution of $10^9 M_\odot$ corresponds to the entire one-zone system being represented with a single particle with all clouds interactions modelled with the coagulation equations.

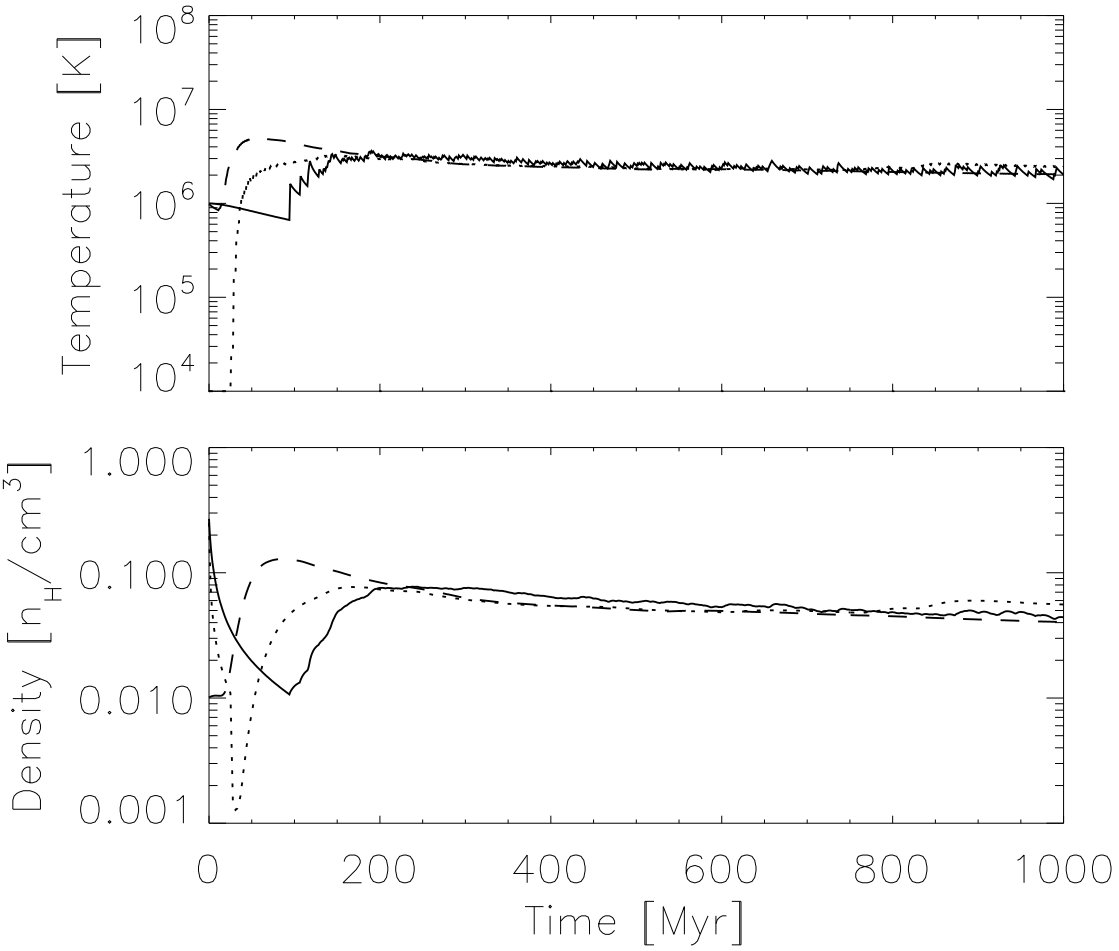

Figure 3.9: Temperature and density of the ambient phase of a one zone model for a variety of different choices of initial temperature and density. The total gas density, ambient gas plus clouds, is always 2 cm^{-3}. The interplay of supernova feedback and radiative cooling quickly brings the system into an equilibrium independent of the initial value. The initial conditions for each of the simulations are as follows: $T = 10^6 K$, 100% atomic (solid line); $T = 10K$, initially 100% atomic (dotted line); $T = 10^6 K$, initially 10% atomic (dashed line).

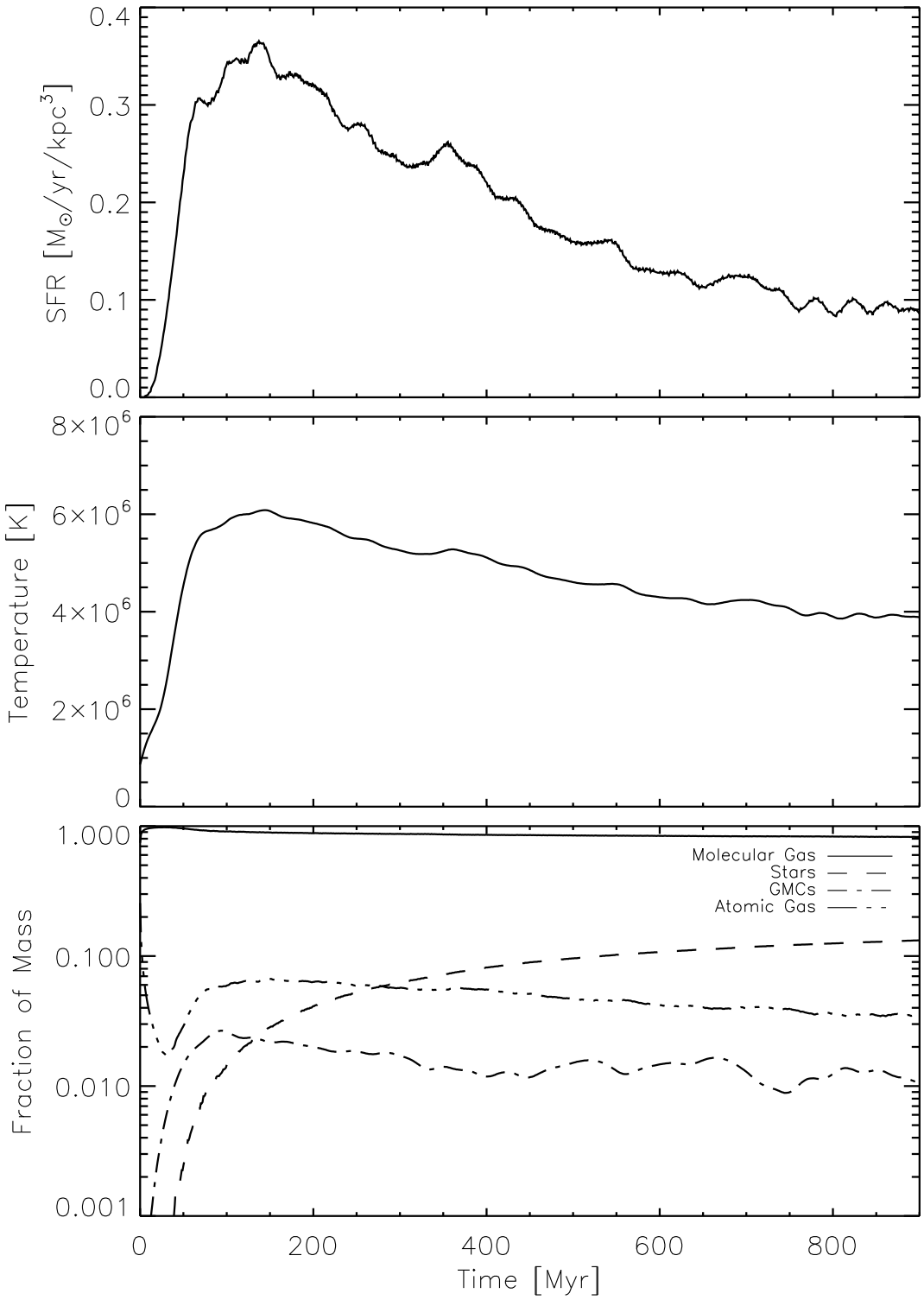

Figure 3.10: The large scale properties of a one zone model with initial density $n_0 = 2$ cm^{-3}. The physical parameters used in this model are the same as the base model as discussed in section 3.3.1

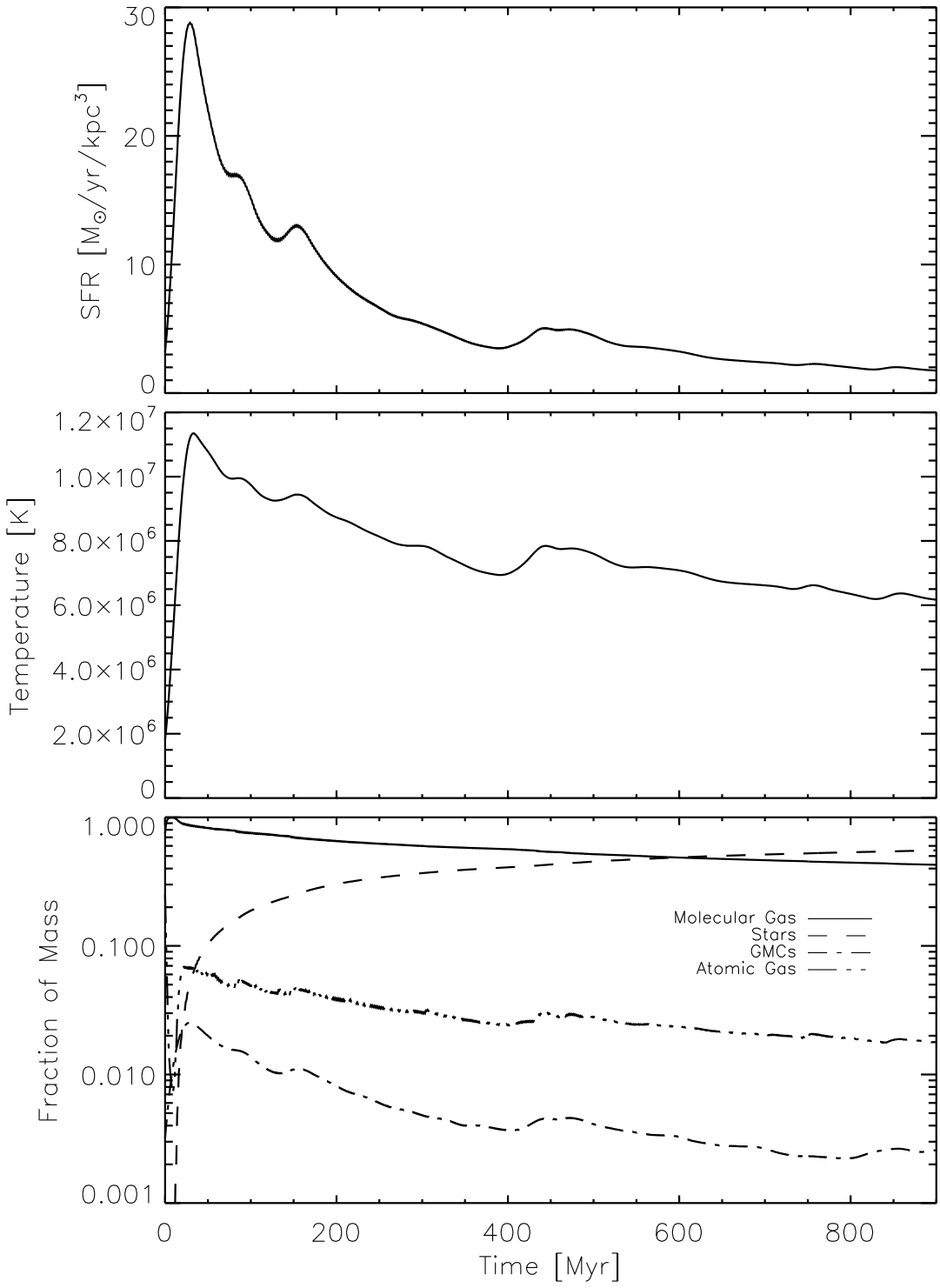

Figure 3.11: Same as Fig (3.10) except with an initial gas density of $n_0 = 16\ \mathrm{cm}^{-3}$

relation, α_c; the efficiency of star formation in any given cloud collapse, $\epsilon_\star$; the maximum relative cloud velocity for merger ($v_{\rm stick}$) and the amount of energy ejected per SNII event (E_{51}).

Even though the initially assumed cloud spectrum, $N(M)dM \propto M^{-8}\,dM$, is very steep and far from equilibrium, SNe feedback and cloud coagulation rapidly build a mass spectrum $N(M)dM \propto M^{-\alpha}\,dM$ with $\alpha \approx 2$ (Fig (3.6)), close to what is the observed cloud spectrum in the MW (dashed line) and M33 (dotted lines). This gives us confidence that, although the modelling of cloud formation is simple, it does produce a realistic cloud spectrum.

The ISM model can also reproduce the observed Schmidt law. We find that in our model the interaction between the coagulation of clouds and their destruction by stars leads to a SFR-density relation that is in good agreement with observation (Fig (3.7)) if $v_{\rm stick}$ is set to 7km/s. This represents a reasonable value for the molecular cloud velocity dispersion, as considering theoretical models for the origin of random motion on molecular clouds, we would expect typical velocities in the range 5-7km/s (Jog and Ostriker (1988))

The effect of changing the mass resolution of the simulation over two orders of magnitude is demonstrated in Fig (3.8). Sub-resolution clouds that are simulated only by integrating the coagulation equations are designed to behave in exactly the same way as the resolved cloud particles in the simulation, and so we expect the simulations not to depend strongly on particle number. This is borne out by the good agreement between simulations carried out with only one resolved particle (Fig (3.8), line with mass resolution of $10^9 M_\odot$) where all of the physics is followed by integrating the sub-grid equations in a single particle and simulations with a hundred particles that are followed explicitly.

As stated in previous sections, the behaviour of a one zone model is virtually independent of its initial temperature and the fraction of the gas that starts off in the cold phase. This behaviour is demonstrated in Fig (3.9). A one zone volume with total initial density of $n_0 = 2{\rm cm}^{-3}$ was evolved with a variety of different initial values for the initial temperature and initial fraction of the mass in the hot phase. We observe that regardless of the initial choices for these two quantities the system quickly settles down to its equilibrium state. This process occurs through the opposing actions of thermal conduction and supernova feedback.

Fig (3.10) and Fig (3.11) show the behaviour of the large scale properties of two different one zone volumes as a function of time. The only difference in the initial condi-

tions of the two one zone volumes is their initial density Fig (3.10) shows the evolution of a one zone volume with a total density of 2 atoms/cm^3; Fig (3.11) shows exactly the same plots for a density of 16 atoms/cm^3. The initial temperature of the hot phase in both simulations is 10^6K. In both cases the star formation rate follows the same general shape. There is a small period of time at the beginning of the simulation where small clouds are coagulating and there is no star formation. When GMCs are formed there is a large burst of star formation that is quickly quenched by feedback SN and thermal conduction in SN bubbles. The temperature of the diffuse phase is regulated by a combination of supernova feedback (acting to increase the temperature) and radiative cooling. Due to the fact that we do not allow mass to leave the one zone volume and also assume instantaneous recycling, the temperature profile very closely matches that of the star formation rate. It is noted that in the one zone simulation with the largest density, the temperature of the ambient phase is held at a higher temperature by the action of supernovae. The fraction of the gas in the molecular phase is lower in the high density simulation due to the increased amount of evaporation by thermal conduction in the high temperature ambient phase. In the following chapter the star formation and feedback prescriptions are tested in a more realistic situation, and the properties of the ISM in a simulated galaxy are investigated. In the final chapter we look in detail at the star formation history of a merging galaxy.